


ORIGINAL RESEARCH

Open Access



Porous honeycomb cork biochar for efficient and highly selective removal of phosphorus from wastewater

Xiuxiu Jia^{1†}, Tao Yin^{1†}, Yin Wang², Shuxing Zhou^{2*}, Xue Zhao^{3*}, Wentong Chen⁴ and Guangzhi Hu^{1*} 

Abstract

In this study, an adsorbent (LCB) with rich honeycomb structure was prepared from cork waste generated from furniture factories for efficient adsorption of excess phosphorus (P) from wastewater. This adsorbent was successfully prepared in only one step, in situ precipitation method, which greatly simplified the synthesis process. Kinetic studies showed that when the initial concentration (C_0) of wastewater was 10 mg P L^{-1} , the P in the water could be completely adsorbed within 20 min. The adsorption efficiency of phosphorus was significantly improved compared to previous studies. When the C_0 of pollutant and the dosage of LCB were 20 mg P L^{-1} and 0.5 g L^{-1} , respectively, the removal rate of P exceeded 99% in the pH range of 3–10, which indicates the wide applicability of LCB. In addition, the P adsorption capacity of LCB was 82.4% of its initial value after nine adsorption–desorption cycles, indicating that LCB has a high stability and can be widely used in different water environments. Therefore, LCB is a promising material for the treatment of P-containing wastewater.

Article Highlights

- Highly efficient P-absorber with honeycomb structure and high specific surface area ($2093.1 \text{ m}^2 \text{ g}^{-1}$) was prepared.
- LCB had an adsorption capacity of up to $280.4 \text{ mg P g}^{-1} \text{ La}^{-1}$ and its reusability was outstanding.
- LCB maintained good P-removal effect at a solution pH of 3~10 and can be used in a wide range of applications.

Keywords Cork biochar, Phosphorus removal, LCB, Adsorption, Wastewater treatment

[†]Xiuxiu Jia and Tao Yin have contributed equally.

Handling editor: Xiangzhou Yuan

*Correspondence:

Shuxing Zhou

szzhou@hbuas.edu.cn

Xue Zhao

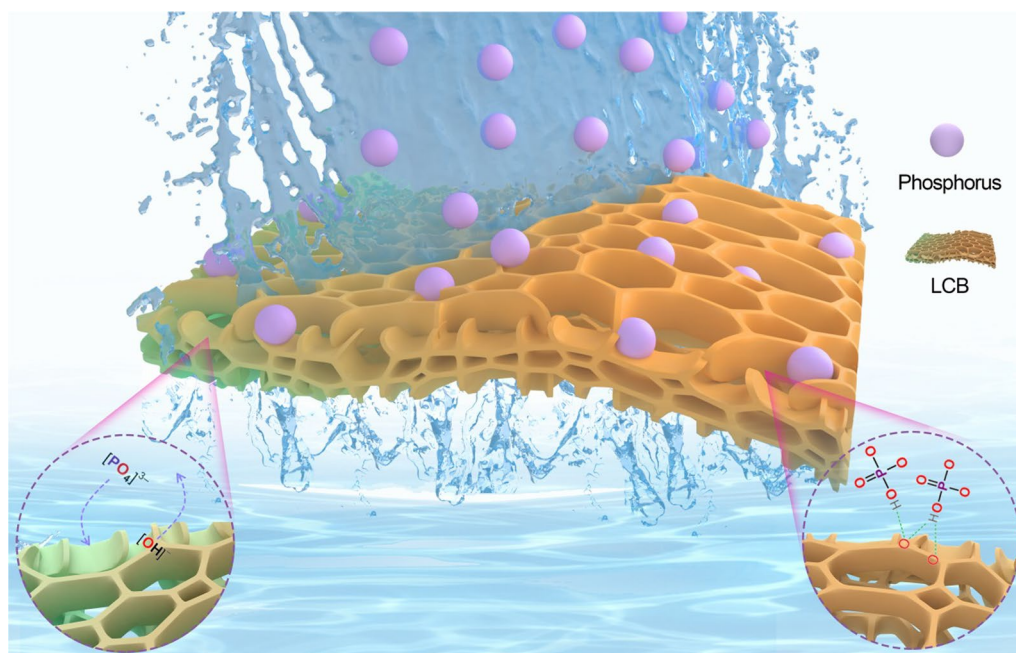
zhaoxue@ynnu.edu.cn

Guangzhi Hu

guangzhihu@ynnu.edu.cn

Full list of author information is available at the end of the article

Graphical Abstract



1 Introduction

Phosphorus (P) is an important nutrient; however, excess P can severely pollute aquatic environments (Cheng et al. 2023; Feng et al. 2023b). For example, it causes excessive algal growth, hinders photosynthesis in aquatic plants, causes the mass mortality of aquatic animals, reduces the number and diversity of aquatic species, and decreases the stability and diversity of aquatic ecosystems (Wang et al. 2023a). In addition, eutrophic water can cause hyperphosphatemia in humans, resulting in osteoporosis (Li et al. 2023b). Scientists have investigated various methods of removing excess P from water to address these issues.

Typical P removal methods include chemical precipitation, in which certain water-soluble metal salts are added to water, and the metal ions react with P to form insoluble salts, thus separating them from water (Lüring et al. 2020). Ion exchange is another method that uses porous anion-exchange resins to selectively absorb and remove P from wastewater (Dong et al. 2020). Biological phosphorus removal technology utilizes the biochemical processes of microorganisms to remove P from water (Sun et al. 2021). Adsorption removes P from wastewater based on the affinity of certain porous or large-surface-area solid materials for phosphate ions in water (Liu et al. 2023). Because the capacity of the adsorbent is limited, it may rapidly become saturated

when the concentration of contaminants in the solution is high, thereby affecting the removal efficiency. Therefore, adsorption is typically preferred for treating water with low P concentrations (Arroyave et al. 2022). The advantages of this adsorption method include its low energy consumption, low pollution, fast removal, and easy recovery. However, it presents some disadvantages, such as the regeneration and treatment of the adsorbent, which may be problematic (Mahata et al. 2022).

The selection of a sorbent depends on many factors, including the contaminant concentration, water quality, treatment goals, and cost. Adsorbents typically used include activated carbon, zeolites, bentonite, and iron oxide (Moumen et al. 2022). However, the adsorption of P by purely environmental mineral materials is either weak or ineffective. Therefore, researchers have used these materials as carriers and loaded them with other metal salts that can react with phosphate ions in water to form insoluble salts for P removal (Wang et al. 2021b). Typical metal salts used for P adsorption include aluminum, iron, lanthanides (La), and complex metal salts. Among them, adsorbents containing La have better removal performance for P. However, in practical applications, La-containing materials exhibit unsatisfactory recoverability and low La utilization. Therefore, suitable carriers should be selected.

Biochar, due to its rich pore structure, high carbon content, and the ability to improve soil fertility, has been widely used as an adsorbent material for P pollutants in water bodies. Several studies have selected various biomass sources to prepare biochar materials for adsorbing excess phosphate in water bodies. This not only removes phosphorus but also facilitates the resourceful reuse of discarded biomass materials, contributing to ecological sustainability, such as Brazil nut shells palm kernel cake (Canteral et al. 2023a), rice husk and corn stover (Zhao et al. 2017), sesame straw (Park et al. 2015), woody materials (Sarkhot et al. 2013), carrot residues (de Carvalho Eufrásio Pinto et al. 2019).

Cork is a natural polymer produced from the bark of subtropical trees. It is produced in large quantities and widely used in the construction and furniture production industries (Zhang et al. 2020). However, the large amount of cork waste generated during furniture production harms the environment and increases the cost of solid waste disposal. Compared to the previously reported biochar-based phosphorus absorbers mentioned above, cork biochar has a high specific surface area (SSA), and its internal structure is a highly ordered arrangement of pentagons or hexagons. They maintain their original structure under high-temperature conditions, making them high-quality carriers (Liu et al. 2022). However, no studies have been reported on applying cork biochar for phosphorus adsorption. Considering the above factors, the use of cork waste can solve the problems of waste reprocessing and the instability of La-loaded adsorbents and reduce the development cost of adsorbents.

Therefore, a new adsorbent, La-loaded cork biochar (LCB) was developed. Because potassium compounds undergo redox reactions with carbon, etch the carbon skeleton, and create pores (Wang and Kaskel 2012), the cork biomass was activated using potassium hydroxide (KOH), which was hypothesized to increase the SSA of the material after activation, thus improving the diffusion rate and adsorption efficiency of P on LCB. In addition, considering that the strong binding capacity between P and metal La, it is hypothesized that loading La on cork biochar can achieve efficient adsorption of P. In this study, the adsorption performance of the adsorbent for P and its influencing factors were investigated, the reaction process and adsorption mechanism between the two were elucidated, and the adsorbent's recovery value and selective adsorption were evaluated. In addition, the effect of the adsorbent on P removal from wastewater was investigated. This study provides a new method for removing P from wastewater and provides more options for the use of adsorbents.

2 Materials and methods

Cork waste was obtained from the Laucork Cork Flooring Plant in Shandong Province, China, which generates approximately 30–40% of the total cork during the preparation of furniture (Demertzi et al. 2016). From a microscopic perspective, cork consists of tightly packed stacks of highly ordered pentagons or hexagons that retain their original structure at high temperatures. In addition, cork biomass contains numerous oxygen-containing functional groups. Secondary utilization of cork waste can solve the problem of reprocessing solid waste, improve the stability of adsorbents, and reduce the development cost of adsorbents.

2.1 Preparation of adsorbents

The cork was cleaned to remove impurities. Subsequently, it was dried and carbonized at 500 °C for 1.5 h under N₂ conditions to obtain the product, which was named CB (Wang et al. 2021a). Next, CB and KOH powders were mixed in ratios of 1:3, 1:4, and 1:5 and then carbonized at 750 °C for 2 h. The impurities inside the product were washed with hydrochloric acid (0.1 M), washed with deionized water to neutral pH, and dried to obtain products CB-1, CB-2, and CB-3. CB-3 was selected for the subsequent preparation because it had the largest SSA. CB-3 and La(NO₃)₃ were dispersed in appropriate water at a 1:1 weight ratio and stirred for 10 h. Subsequently, the pH of the solution was adjusted to 11 using 1 M NaOH, and stirring was continued for 10 h. The obtained solid material was washed with ultrapure water to neutralize the pH and dried to obtain the final product, denoted as LCB. The prepared materials were analyzed by X-ray diffraction (XRD), scanning electron microscopy (SEM), Brunauer–Emmett–Teller (BET) analysis, Fourier transform infrared (FTIR) spectroscopy, and X-ray photoelectron spectroscopy (XPS). The instruments and reagents used in this study are listed in Additional file 1.

2.2 P adsorption experiments

KH₂PO₄ was dissolved in deionized water to prepare a standard P solution with a concentration of 100 mg P L⁻¹; subsequently, it was diluted to the desired concentration. Adsorption reactions were conducted in a constant-temperature shaker (ZHWHY 334, Zhicheng, China). The P and La concentrations were determined using an ultraviolet–visible spectrophotometer (HACH, DR5000, USA) and an inductively coupled plasma mass spectrometer (iCE 3500, Thermo Fisher, USA). All experiments were carried out under the following reaction conditions unless stated separately: temperature, 25 ± 0.5 °C; stirring speed, 150 rpm; adsorption time, 12 h; initial pH of the solution, ~6; initial concentration, 20 mg P L⁻¹;

adsorbent dose, 0.5 g L⁻¹. The amount of adsorbed P was calculated according to the equation provided in the Additional file 1.

2.2.1 Effect of initial solution pH

The pH was adjusted to 2, 2.5, 3, 4, 5, 6, 7, 8, 9, 10, and 11 using HCl and NaOH (0.1 ~ 1 M) to investigate the effect of solution pH on P removal.

2.2.2 Adsorption isotherm

Adsorption isotherm experiments were performed at 288, 298, and 308 K, and at each temperature, the initial solution concentrations were set to 20, 50, 75, 100, and 150 mg P L⁻¹. The Langmuir and Freundlich models were used to fit the LCB process for P adsorption to verify whether the adsorption process was monolayered or multilayered. The fitting equations are listed in Additional file 1: Table S1 in the Additional file.

2.2.3 Adsorption kinetics

Kinetic experiments were performed at 10, 20, and 50 mg P L⁻¹ initial concentrations. The samples were obtained at specific intervals (i.e., 10 mg P L⁻¹: 1, 2, 5, 10, 15, and 20 min; 20 mg P L⁻¹: 2, 5, 10, 20, 60, 100, and 150 min; and 50 mg P L⁻¹: 5, 10, 20, 40, 60, 100, 150, 240, 360, and 480 min). Pseudo-first- and pseudo-second-order kinetic models were used to fit the reaction process and verify whether the adsorption process involved physisorption or chemisorption. The fitting equations are listed in Additional file 1: Table S1 in the Additional file.

2.2.4 Effects of coexisting ions

To investigate the competitive adsorption of P based on typical anions in binary systems, such as Cl⁻ (KCl), NO₃⁻ (KNO₃), CO₃²⁻ (K₂CO₃), and SO₄²⁻ (K₂SO₄), different concentrations of competing ions were specified, i.e., 50, 100, and 200 mg L⁻¹ because the ion concentrations in natural water vary.

2.2.5 Reusability of adsorbent LCB

To verify the reusability of the adsorbent, 1 M NaOH was used as the desorbent for LCB. After the adsorption of P, 2 g of the LCB was stirred in 1 L of NaOH solution for 10 h, washed with deionized water until neutral, and dried in an oven. The adsorption–desorption process was repeated nine times.

2.2.6 Data analysis

The P-removal performance of the LCB was investigated using batch performance experiments. All experimental data were obtained in triplicate, and the results were reported as the average and standard deviation. The software origin was used to statistically analyze the

experimental data. The Shapiro–Wilk test was used to derive the normal distribution of the validation data, and the output was considered non-normally distributed if the significance level was below the set value (*p*, usually set at 0.05) for the resulting dataset (Canteral et al. 2023b). A one-way analysis of variance (ANOVA) was applied to investigate the level of control factors for the target variables and the significance of their effects.

3 Results and discussion

3.1 Material characterization

As shown in Table 1, the SSA of CB calculated using the calculation model (Langmuir monolayer adsorption equation) was 73.27 m² g⁻¹. The SSA of CB-1, CB-2, and CB-3 were 2093.11, 2712.40, and 3504.60 m² g⁻¹, respectively. The significant increase in the SSA can be attributed to the following reasons. First, P compounds react with carbon through redox to etch the carbon skeleton and create pores. Second, metallic P can develop effectively in the carbon lattice of the carbon substrate, causing the carbon lattice to swell. Washing away metallic P or P compounds generates numerous microporous structures in the swollen carbon lattice (Wang and Kaskel 2012). Therefore, CB-3 was selected as the biochar carrier for La loading in this study. The SSA decreased after loading because some La(OH)₃ products obstructed the pores inside the LCB. Figures 1b, d, and f show that CB exhibited the characteristics of a type-IV isotherm, indicating a mesoporous structure. Meanwhile, CB-3 and LCB exhibited type I and type IV isotherm characteristics, indicating that they were microporous-mesoporous composite materials (Feng et al. 2023a; Sing 1985). The pore size distribution plots (Figs. 1 c, e, and g) show that they mainly consisted of microporous structures with a few mesopores larger than 2 nm, which verified the N₂ adsorption/desorption curve results. Hence, the LCB contained both micro-sized macropores, numerous micropores, and a few mesopores, which can improve its

Table 1 Pore structure parameters of materials used in current study

Adsorbent	SSA (m ² g ⁻¹)	V _{tot} ^a (cm ³ g ⁻¹)	V _{mic} ^b (cm ³ g ⁻¹)	V _{mic} /V _{tot} (%)	Pore size (nm)
CB	73.27	0.06	0.02	33.33	5.29
CB-1	2460.81	0.92	0.82	89.13	2.21
CB-2	2712.40	0.99	0.92	92.92	2.10
CB-3	3504.60	1.25	1.12	89.60	2.15
LCB	2093.11	0.89	0.57	64.04	2.66

SSA specific surface area

^a total

^b micropore

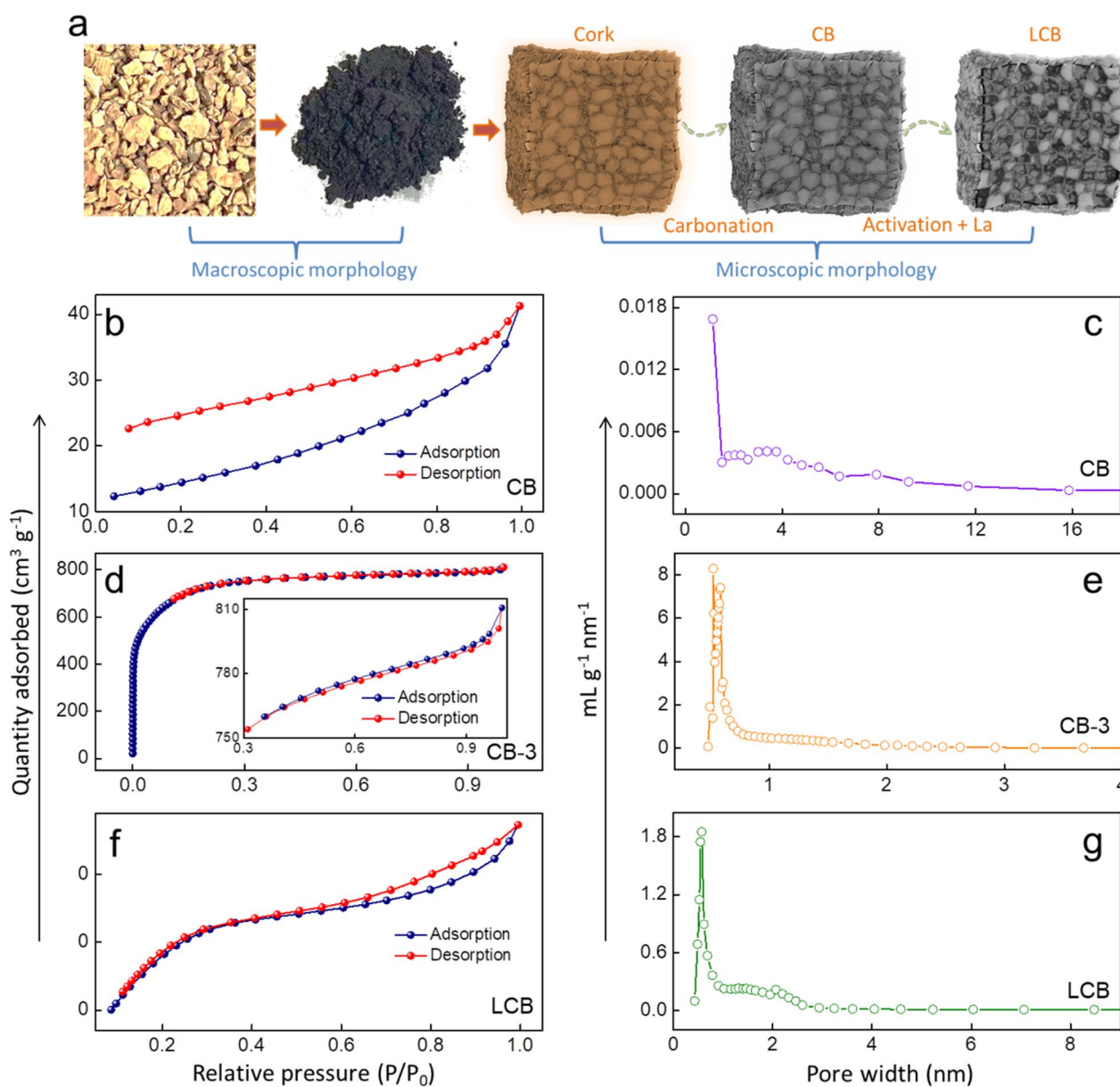


Fig. 1 a Scheme illustration of the preparation of adsorbent; **b, d, f** N₂ adsorption/desorption curves of CB, CB-3, and LCB; **c, e, g** Pore size distributions of CB, CB-3, and LCB

diffusion rate and P-adsorption efficiency. Table 1 lists the pore structure parameters of the materials used in this study.

The XRD pattern of the LCB is shown in Fig. 2a. The diffraction peaks at diffraction angles (2θ) of 27.97°, 39.48°, 27.31°, and 48.64° matched the (101), (201), (110), and (211) crystallographic planes of La(OH)₃ on the standard card JCPDS No.36–1481 (Jia et al. 2023b), thus indicating that La(OH)₃ was produced on LCB and that the sample was of high purity. After adsorbing P, the diffraction peaks at 2θ values of 28.52°, 30.89°, 26.78°, and

48.13° matched the (120), (012), (200), and (–132) crystal planes of LaPO₄ on the standard card JCPDS No.32–0493, thus indicating that P reacted with La in LCB to form LaPO₄.

FTIR spectra of the LCB composite before and after P adsorption are shown in Fig. 2b. A broad peak appeared at 3425 cm⁻¹, which was caused by the bending vibrations of water adsorbed on the material surface or the vibrations of the H–O–H functional group on La(OH)₃ (Glemser 1959). The absorption peaks at 1384 and 1477 cm⁻¹ corresponded to the stretching vibrations of

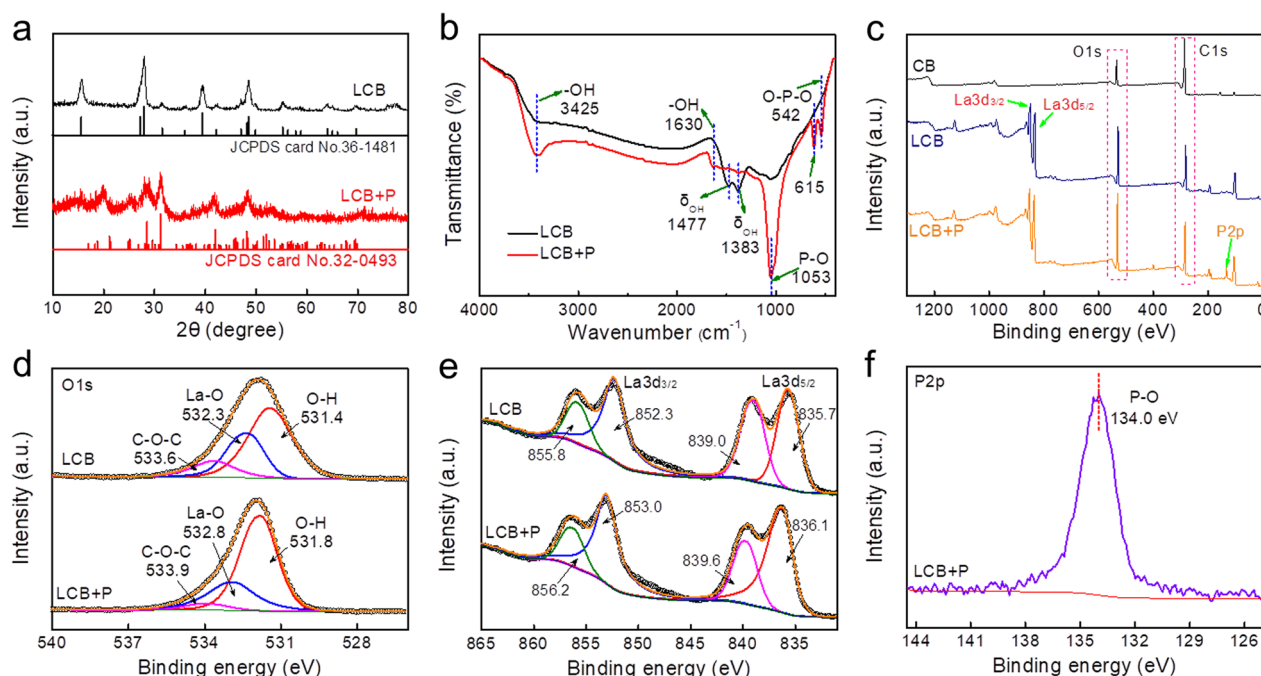


Fig. 2 a XRD patterns of LCB and LCB + P; b FT-IR spectra of LCB and LCB + P; (c) XPS spectra of LCB and LCB + P; high-resolution XPS spectra of d O 1 s, e La 3d, and f P 2p

the primary alcohol δ_{OH} on the surface of the LCB. Several new vibrational peaks were observed for LCB after P adsorption. A P-O stretching vibration peak appeared at 1053 cm^{-1} and a shoulder peak at 1016 cm^{-1} , belonging to the ν_3 vibration of the PO_4^{3-} group. The absorption peaks at 615 and 542 cm^{-1} corresponded to the ν_4 vibration of the phosphate group (Yu et al. 2019). The peak at 1630 cm^{-1} was attributed to the -OH stretching vibration of H_2PO_4^- (Shan et al. 2021). The appearance of these vibration peaks confirms that the LCB successfully adsorbed the P species. Simultaneously, the -OH bending vibration peaks at 1384 and 1477 cm^{-1} disappeared entirely for several flats, proving the -OH's involvement in the reaction.

The total XPS spectrum (Fig. 2c) shows that, after the adsorption of P, a P 2p signal peak was detected on the LCB, indicating that the LCB successfully adsorbed P. Figure 2f shows that the characteristic peak of P 2p appeared at 134.0 eV , which is consistent with the spectrum of KH_2PO_4 ($\sim 134.0 \text{ eV}$) (Shan et al. 2021), thus indicating that P was bound to LCB in the form of phosphate and did not change its morphology. The signal peaks at 835.7 and 852.3 eV in Fig. 2e corresponded to La $3d_{5/2}$ and La $3d_{3/2}$ with a spin-orbit splitting energy of 16.6 eV , respectively, and their satellite peaks were indicated at 839.0 and 855.8 eV , respectively (Shan et al. 2020). The La 3d peak of LCB shifted toward a higher binding energy after P adsorption, which indicates that the P ions may react

with the La-O functional group on the surface of LCB to form the LaPO_4 inner sphere complex; the decrease in the La-O functional groups in LCB from 30.1% to 27.8% indicates its participation in the adsorption reaction. The formation of such complexes facilitates the immobilization of P ions on the adsorbent to remove pollutants from the water column.

Figures 3a, b show the SEM images of the CB and LCB, respectively. CB featured a natural honeycomb structure comprising several relatively regular pentagons or hexagons with an average size of $\sim 25 \mu\text{m}$ and a diverse pore structure, thus rendering it suitable as a precursor for modified adsorbent materials. The LCB maintained the contour structure of the CB, although the membrane at the bottom of the honeycomb cell cracked, allowing the pores to connect. Hence, the specific surface area of the LCB was much larger than that of the CB. The higher specific surface area facilitates the diffusion of P from the solution to the interior of the LCB, thus increasing the number of adsorption sites and promoting the efficient adsorption of P. The cell wall thickness of the LCB honeycomb structure was $\sim 0.8 \mu\text{m}$, which presents the structural characteristics of a nanosheet. The elemental profiles after the adsorption of P are shown in Figs. 3f-j. A comparison with the mapping plot of the LCB showed that the P signal appeared uniformly on the LCB, indicating that P was successfully adsorbed onto the LCB. The TEM image of the LCB shows a large number of

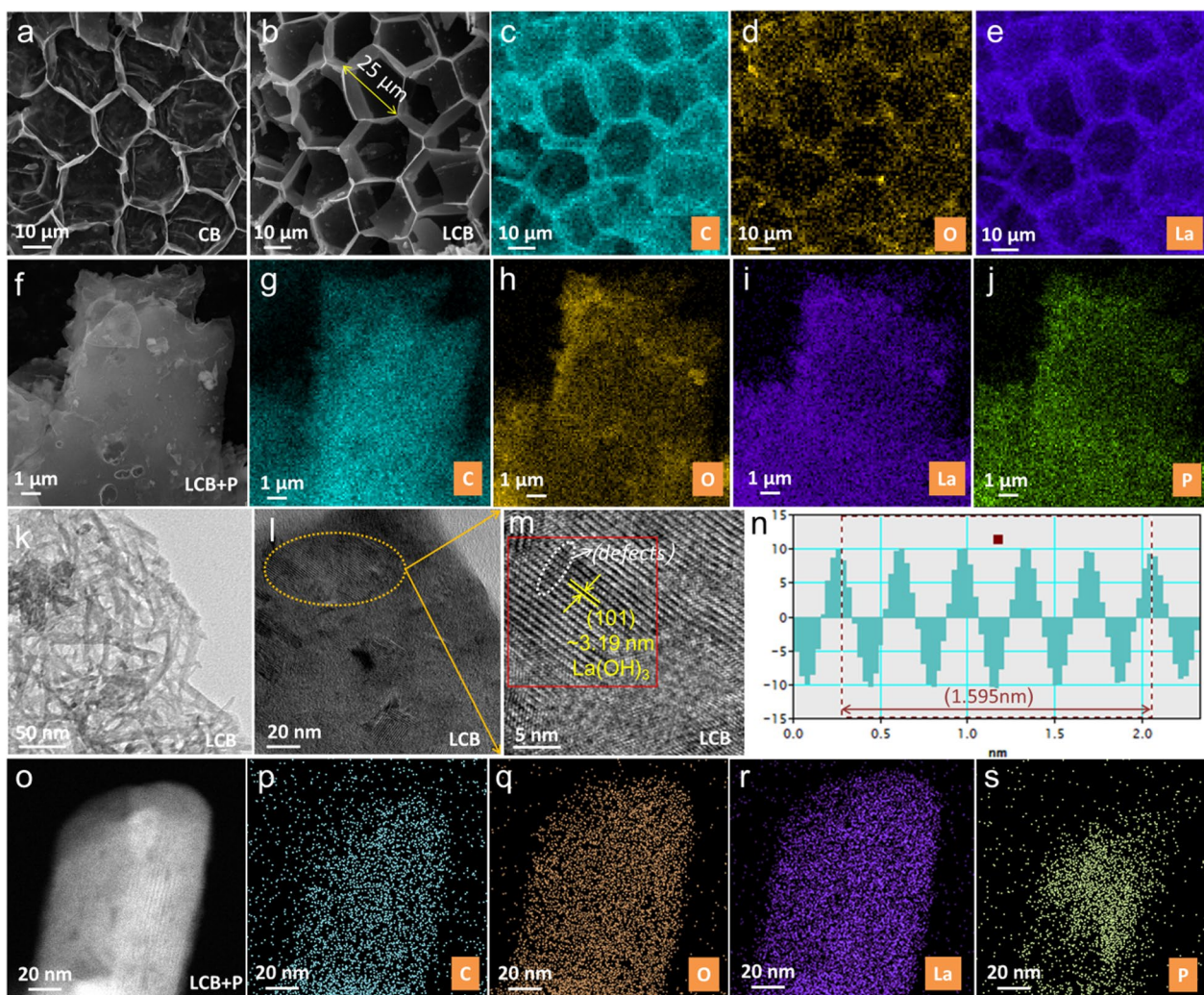


Fig. 3 a SEM images of CB; SEM images and EDS mapping of LCB (b–e) and LCB+P (f–j); TEM images of LCB (k–n) and LCB+P (o–s)

longitudinal and transverse nanorods, and the lattice stripe spacing in Figs. 3m, n analyzed by the DM software is consistent with that derived from the XRD standard spectra, indicating that this rod-like structure represents $\text{La}(\text{OH})_3$. As shown in Fig. 3m, the surface lattice of the LCB exhibited deformation defects. The construction of defects is considered to play an essential role in enhancing the activity of the adsorbent because it can effectively increase the number of active sites and improve their activity of the active sites (Huang et al. 2023; Lin et al. 2019). The mapping profile of the LCB after P adsorption (Figs. 3o–s) derived by TEM also detected the signal of P, which is consistent with the SEM analysis.

3.2 Effect of initial solution pH

Figure 4a shows that the phosphorus uptake of LCB increased and decreased with an increase in the pH of the solution. At $\text{pH} \leq 2.15$, the P in the solution appeared

mainly in the form of H_3PO_4 molecules (Li et al. 2021), which inhibited effective contact between P and LCB, thus resulting in a lower removal rate. When the pH was between 3 and 10, the adsorption capacity of the LCB was 39.9 mg P g^{-1} at an initial concentration of 20 mg P L^{-1} and an adsorbent dosage of 0.5 g L^{-1} . The P removal rate exceeded 99.9%, indicating that the LCB extract can be effectively utilized over a wide pH range.

At pH values exceeding 10, the significant increase in $-\text{OH}$ in the solution eventually weakened ligand exchange (Li et al. 2023a). However, based on the zeta potential test (Fig. 4b), the isoelectric point of the LCB was 8 (Fig. 4b). This indicates that when the pH of the solution is less than 8, the surface of the LCB is positively charged due to protonation, which causes it to be electrostatically attracted to the negatively charged phosphate ions, resulting in P removal (Zhang et al. 2022).

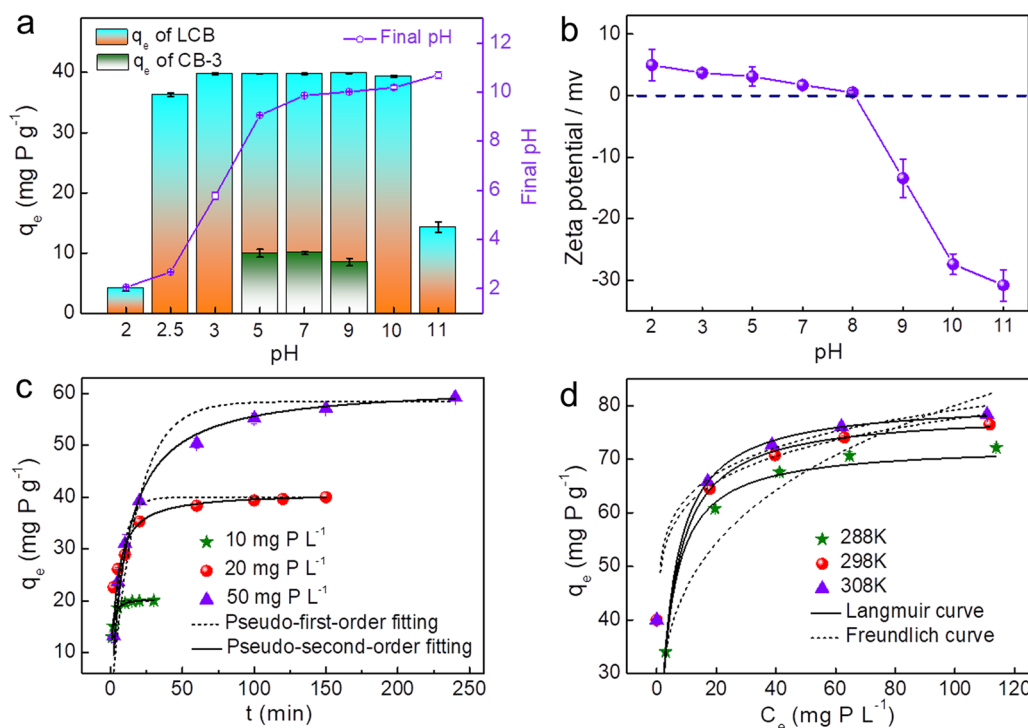


Fig. 4 **a** Effect of solution pH (20 mg P L⁻¹; 298 K; contact time: 3 h); **b** zeta potential of LCB; **c** adsorption kinetic models of LCB toward P; **d** adsorption isotherm models of LCB toward P (25, 50, 75, 100, and 150 mg P L⁻¹). LCB dosage: 0.5 g L⁻¹

Table 2 La leakage from LCB at different pH values

pH	2	2.5	3	5	7	9	10	11
Leaching of La	103.2 mg L ⁻¹	65.8 mg L ⁻¹	132.4 μg L ⁻¹	0.3 μg L ⁻¹	1.2 μg L ⁻¹	1.4 μg L ⁻¹	8.9 μg L ⁻¹	22.7 μg L ⁻¹

This proves that ligand exchange is vital for adsorption when the solution pH exceeds 8.

To verify the stability of LCB, the leaching of La from the LCB was examined under different pH conditions. As shown in Table 2, lanthanum leaching was greater when the solution pH was <3, indicating that the adsorbent was less stable under strongly acidic conditions. La leaching was below 150 g L⁻¹ at pH values between 3 and 11, which is the maximum concentration of total La allowed by Dutch law in freshwater (van Oosterhout et al. 2020). In summary, when the pH of the solution was 3–10, the removal rate of P could reach 99.9%, and the stability of the LCB was high, indicating that it has a wide range of applications.

3.3 Adsorption kinetics

Figure 4c shows that the P adsorption rate was initially high and then decreased; the reaction stabilized when the adsorption sites on the LCB were fully occupied. When

C₀ was 10, 20, or 50 mg P L⁻¹, the adsorption reactions stabilized at 20, 150, and 480 min, respectively, indicating high adsorption rates. The BET characterization results showed that LCB featured a diverse pore structure, which can improve the diffusion rate and P adsorption efficiency of LCB.

The relevant parameters fitted using the two kinetic models are listed in Table 3. The fitting coefficient (R²) of the pseudo-second-order kinetic model was higher than that of the pseudo-first-order kinetic model. The theoretical adsorption amounts q_e (20.0, 40.0, and 61.7 mg g⁻¹) fitted by the pseudo-second-order kinetic model were more similar to the experimentally derived values (20.0, 40.0, and 63.6 mg g⁻¹) than those fitted by the pseudo-first-order kinetic model. Therefore, the latter is more consistent with the adsorption process, and the primary adsorption mechanism is chemical adsorption (Jia et al. 2022).

Table 3 Parameters of different adsorption kinetic models

C_0 (mg P L ⁻¹)	$q_{e,exp}$ (mg P g ⁻¹)	Pseudo-first-order model			Pseudo-second-order model		
		$q_{e,cal}$ (mg P g ⁻¹)	k_1 (min ⁻¹)	R^2	$q_{e,cal}$ (mg P g ⁻¹)	k_2 (g mg ⁻¹ .min ⁻¹)	R^2
10	20.0	20.6	0.083	0.943	20.0	0.992	0.991
20	40.0	40.9	0.007	0.837	40.0	0.154	0.956
50	63.6	58.5	0.001	0.953	61.7	0.057	0.987

3.4 Adsorption isotherm

Standard adsorption isotherm models include the Langmuir, Freundlich, Temkin, and BET models (Neolaka et al. 2020). Langmuir and Freundlich models are more commonly used in liquid phase adsorption studies. The Langmuir and Freundlich models are commonly used in liquid-phase adsorption studies. The BET adsorption isotherm is an adsorption isotherm model based on the Brunauer–Emmett–Teller equivalent adsorbent surface area and the Langmuir model, which is mainly used in the field of gas adsorption (Erdogan 2019), and is therefore not suitable for our study. The Temkin model is mainly used for the proposed adsorption isotherm model based on its non-conformity with the Langmuir model (Lu and Na 2022).

The Langmuir and Freundlich adsorption isotherm models were used to fit the P adsorption process of the LCB. Figure 4d shows the fitting curves of the two models for different initial P concentrations. The Langmuir model exhibited a higher degree of fit. Table 4 shows that the Langmuir model’s fitting coefficients (R^2) were all greater than 0.99, slightly better than those of the Freundlich model. In addition, the theoretical maximum adsorption capacities obtained from the Langmuir model were almost identical to the actual measured values. *Reduced Chi-Sqr* indicates the degree of direct difference between the experimental and fitted values, the ratio of the *Chi-Square Test* (χ^2), and the *degrees of freedom* (DOM). Therefore, this value can be used to indicate the fitting error of different models, thus corroborating the calculated coefficient of determination results. In nonlinear fitting, the closer the value of *Reduced Chi-Sqr* is to 1,

the better the fit. Therefore, the Langmuir model is more suitable for describing the adsorption of P by the LCB, which suggests monomolecular layer adsorption. In contrast, the diverse pore structures inside the LCB facilitate P passage, thus rendering it more active and enhancing its removal efficiency.

3.5 Comparison with other adsorbents

Currently, most commercial P-removing agents are flocculants that achieve P removal through flocculation and precipitation, whereas fewer P adsorbents are commercially available. La-modified bentonite, developed by the Commonwealth Scientific and Industrial Research Organisation (CSIRO, Australia), is a widely used commercial P adsorbent but still faces the disadvantage of low adsorption capacity (~10 mg P g⁻¹) (Zhang et al. 2021). Some of the reported La-based adsorbents are listed in Table 5. Compared with them, LCB had a wide effective pH range and a significant advantage in phosphorus adsorption capacity, which also indicates the potential of LCB towards commercial phosphorus adsorbent materials.

3.6 Effects of coexisting ions

Wastewater typically contains various anions. When the pH of the solution was below the isoelectric point of the adsorbent, the surface of the LCB was positively charged, which allowed it to interact electrostatically and gravitationally with any anion, including phosphate, to form outer-sphere complexes, thus resulting in competition for P adsorption (Huang et al. 2022). As shown in Figs. 5a, b, when the concentration of competing ions

Table 4 Parameters of different isotherm models

T (K)	$q_{e,exp}$ (mg P g ⁻¹)	Langmuir				Freundlich			
		K_L (L mg ⁻¹)	q_{max} (mg P g ⁻¹)	R^2	<i>Reduced Chi-Sqr</i>	K_F (mg ⁽¹⁻ⁿ⁾ .L ⁿ g ⁻¹)	n	R^2	<i>Reduced Chi-Sqr</i>
288	73.6	0.296	72.7	0.998	8.5	26.5	4.2	0.929	253.1
298	75.3	0.251	76.1	0.991	0.6	48.4	9.6	0.971	1.9
308	80.2	0.256	78.3	0.995	0.8	49.8	9.9	0.963	6.3

Table 5 Comparison with other adsorbents

Adsorbent	pH	Adsorbent dosage (g L ⁻¹)	q _e (mg P g ⁻¹)	Ref
LCNFS	2–7	-	20.2	(Zhang et al. 2016)
MFC@La(OH) ₃	6.5–7	1	45.5	(Liu et al. 2018)
Mag-MSNs-42%La	4–11	0.5	54.2	(Chen et al. 2019)
LPC@La(OH) ₃	3–7	1.25	31.9	(Liu et al. 2019)
La(OH) ₃ -C ₃ N ₄	4–11	1	48.4	(Yin et al. 2022)
LPS	4–10	0.6	50.4	(Jia et al. 2022)
PVDF-La(OH) ₃	2–7	1	58.9	(Wang et al. 2022b)
LAB	3–6	0.5	70.3	(Wang et al. 2022a)
ML2-CGCS	3–8	1.4	39.2	(Wang et al. 2016)
3D La-CA	2–7	1	54.4	(Wang et al. 2023b)
LaATP/CS-0.1	3–9	1	114.1	(Kong et al. 2023)
LCB	3–10	0.5	78.3	This work

was in 200 mg L⁻¹, Cl⁻, F⁻, and SO₄²⁻ had little effect on the P removal of LCB, with inhibition rates of 2.4%, 2.7%, and 4.2%, respectively. Among the four typical anions, only the presence of CO₃²⁻ inhibited the adsorption of P by the LCB because La₂(CO₃)₃ has a lower solubility product constant than LaPO₄ and thus binds more readily to La³⁺. However, even when the concentration of CO₃²⁻ reached 200 mg L⁻¹, the P removal efficiency of the LCB was 87.3% of its original level, which indicates that the LCB had a high selectivity for P adsorption, surpassing that of most reported P adsorbents (Jia et al. 2023a; Shi et al. 2019).

3.7 Reusability of LCB

The regenerative capacity of an adsorbent is critical because it directly affects cost. Therefore, the regenerative performance of the LCB was investigated. The P removal capacity of the LCB decreased at higher pH values, and the final pH value increased after adsorption, which indicates that under highly alkaline conditions, the concentration of OH⁻ is high, and the LCB may undergo desorption and release the adsorbed P back into the solution. Therefore, 1 M NaOH was used as the desorbent.

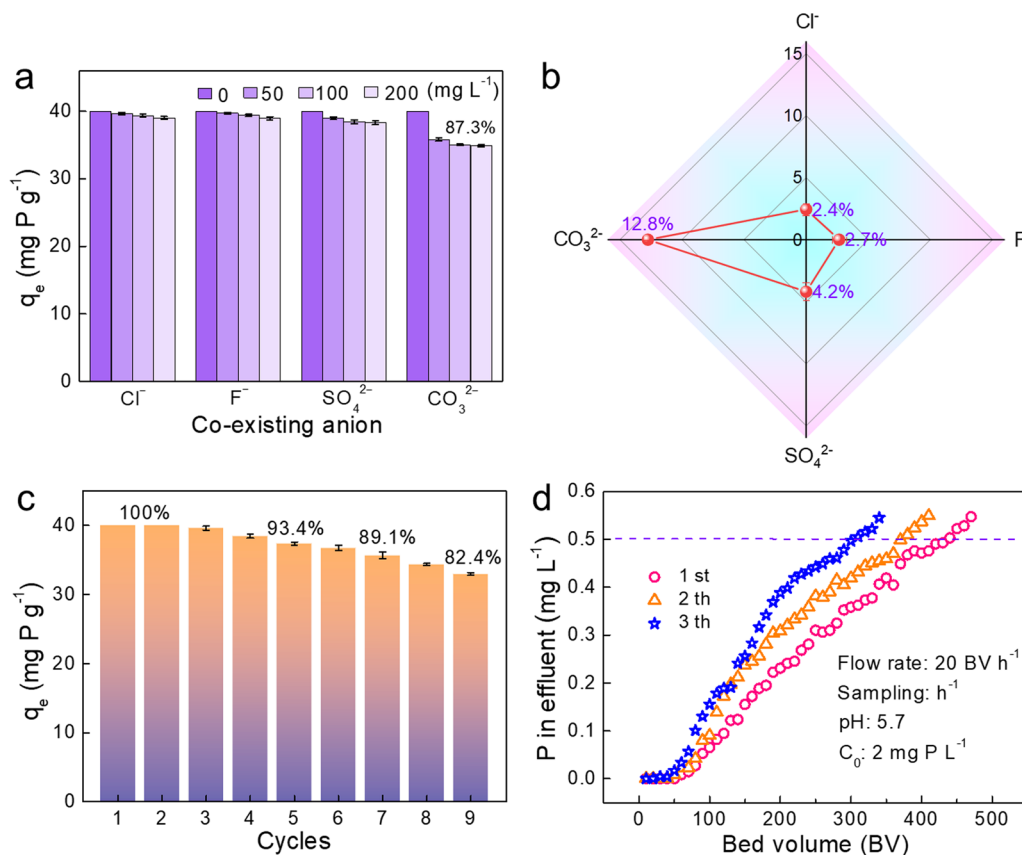


Fig. 5 a Effect of co-existing anions on P adsorption; b Inhibition of P-removal by the presence of competing ions; (Experimental conditions: 298 K; 20 mg P L⁻¹; 3 h; 0.5 g L⁻¹). c Recycling of LCB under static conditions; d Fixed bed experiment

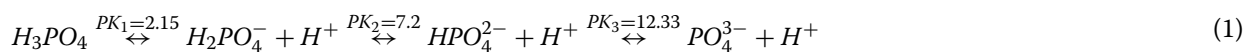
As shown in Fig. 5c, after the ninth adsorption–desorption cycle, the adsorption capacity of LCB was 82.4% of its initial capacity, indicating that LCB exhibited satisfactory regenerative performance, surpassing that of most reported P adsorbents (Feng et al. 2021; Tao et al. 2022).

3.8 Fixed-bed column adsorption experiment

The effectiveness of the LCB in removing low concentrations of P in a continuous flow was evaluated using a fixed-bed column adsorption experiment. The inorganic glass column was filled with a mixture of LCB and quartz sand, which was tested in advance due to quartz sand's lack of P adsorption. The quartz sand and LCB sizes were 80–120 mesh and 100 mesh, respectively. The column volume was 30 cm³; therefore, the volume of one bed (BV) in this experiment was 30 mL. A 2 mg P g⁻¹ solution was prepared as the feed liquid, and a peristaltic pump (Longer-DG15-24) was used to control the feed flow rate at 20 BV h⁻¹. Samples were taken every 0.5 h until the breakthrough point was reached, 0.5 mg P g⁻¹, which is the primary discharge standard for TP in the effluent of wastewater treatment plants as stipulated in the Discharge standard of pollutants for municipal wastewater treatment plants (<0.5 mg P L⁻¹, P element, GB 18918–2002, China) set by China (Shan et al. 2020). When the P content of the effluent reached the breakthrough point, the filler in the column was desorbed *in situ* for 8 h, and NaOH (1 M) was used as the desorbent.

Figure 5d shows that the first fixed-bed experiment could effectively treat 430 BV of P-containing wastewater; 1 g of LCB could treat ~26 L. The second and third

was greater than the repulsive force, and the P species were adsorbed. When the pH of the solution is higher than the isoelectric point of the adsorbent, the surface of the adsorbent is generally electronegative. The electrostatic repulsive effect of negatively charged phosphate is greater than the gravitational effect, and the adsorption between the two is inhibited, resulting in a lower adsorption efficiency (He et al. 2023). The isoelectric point of the LCB was determined to be 8. However, LCB still exhibited a high P adsorption efficiency when the initial pH of the solution ranged from 8 to 10, which indicates that other forces were involved in the adsorption process of P by LCB, namely ligand exchange. The surface of the metal-based adsorbent (metal oxide or metal hydroxide) is occupied by numerous surface hydroxyl (–OH) groups, as shown in the FTIR spectrum in Fig. 2b. In the ligand-exchange process, phosphate ions form covalent bonds with metal ions on the surface of the LCB, which causes the –OH component previously bound to the metal ions to be replaced by phosphate ions (Wang et al. 2023a), resulting in their release into the solution, which explains the increase in the pH of the remaining solution compared to that of the initial solution after the adsorption process (Fig. 4a). The adsorption mechanism involved hydrogen bonding, and the FTIR results showed that the LCB contained numerous hydroxyl functional groups that interacted with phosphate. LCB bound to phosphate by accepting or providing hydrogen bonds; however, hydrogen bonds are generally weaker than the formation of inner complexes during ligand-exchange interactions (Moumen et al. 2022). Fig. 6 shows the P-adsorption mechanism of the LCB.



most effective treated water volumes were 370 and 300 BV, 86.0% and 69.8% of the initial volume, respectively. Dynamic adsorption–desorption experiments better reflect the real situation of LCB applications in actual water bodies. Compared with the static adsorption–desorption experiment in Fig. 5c, the number of recycling cycles and removal efficiency of LCB decreased; however, the adsorbent, LCB, was still very competitive compared with similar studies (Wang et al. 2020; Yin et al. 2022).

3.9 Adsorption mechanism

The P species appeared in the form of anions when the solution pH exceeded 2.15, as shown in Eq. 1. When the pH of the solution was lower than the isoelectric point of the adsorbent, its surface was electropositive, the attractive force between the adsorbent and the phosphate ions

4 Conclusions

This study used cork waste generated by the wood furniture manufacturing industry as a biomass material to adsorb P from wastewater. The diverse honeycomb pore structure of the cork suggests that it can serve as an excellent carrier material. After activation by KOH, the specific surface area of CB increased by approximately 30 times, which can provide a reference value for increasing the SSA of materials. The LCB exhibited a high P removal rate (>99.9%) in the initial solution (pH 3–10), indicating its wide applicability. The maximum adsorption capacity of LCB for P was 80.2 mg P g⁻¹ (280.4 mg P g⁻¹ La⁻¹). In addition, the results of up to nine cycles of adsorption–desorption reuse experiments and the adsorption effect of P in actual wastewater indicate the high practical application prospects of LCB. In summary, an adsorption and P removal reaction system was established in this

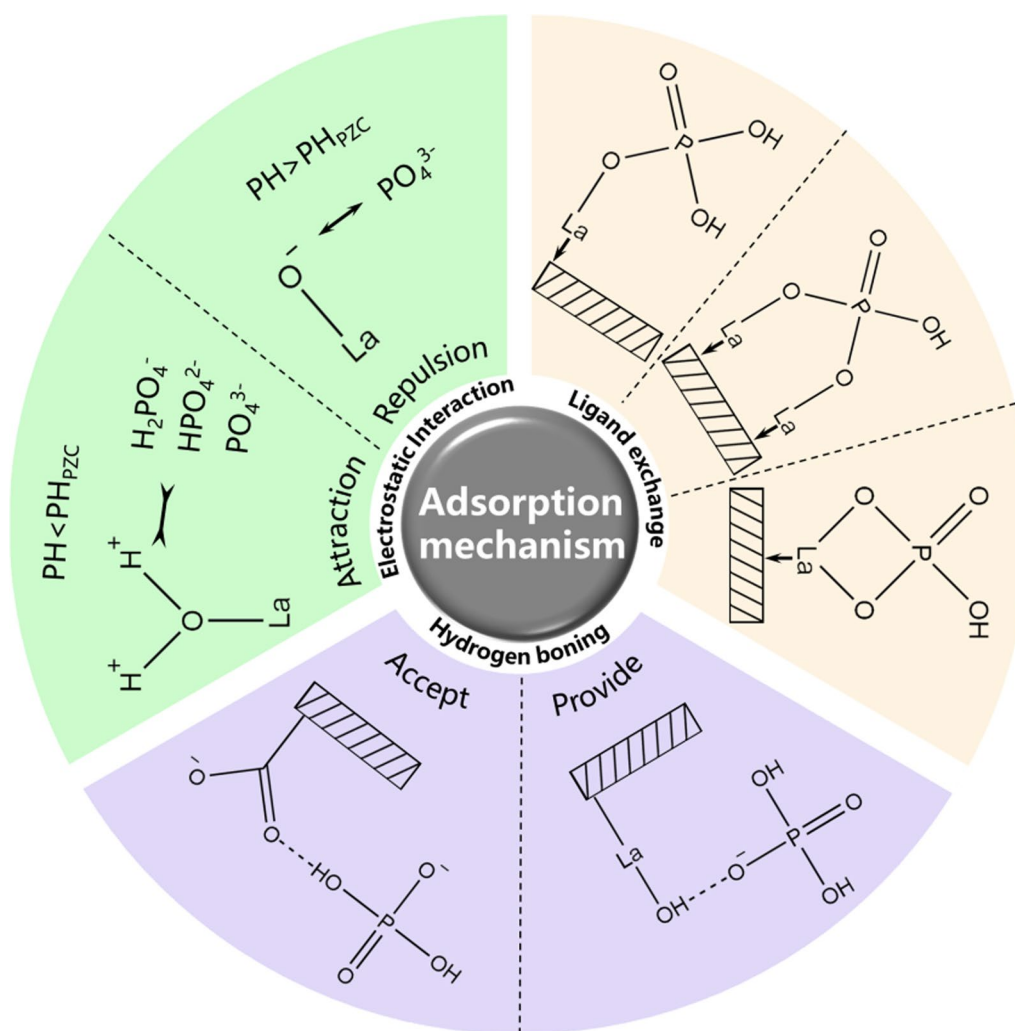


Fig. 6 Adsorption mechanism of LCB for P removal

study based on an LCB with a porous honeycomb structure, which provides technical support for the synthesis of new adsorbents and P removal from wastewater.

Supplementary Information

The online version contains supplementary material available at <https://doi.org/10.1007/s42773-023-00289-9>.

Additional file 1: Table S1. List of calculation formulas and models used in this study.

Acknowledgements

The authors are grateful to the editor and the anonymous reviewers for their valuable comments and constructive suggestions.

Author contributions

XJ Conceptualization, Investigation, Data curation, Writing—original draft. TY Investigation, Data curation. YW Methodology, Formal Analysis. SZ Resources, Writing—review and editing. XZ Validation, Formal Analysis, Writing—review and editing. WC Methodology, Investigation. GH Supervision, Validation,

Funding acquisition, Project administration, Writing—review and editing. All authors read and approved the final manuscript.

Funding

This work was financially supported by the National Key R&D Program of China (2019YFC1804400), Special Project for Social Development of Yunnan Province (202103AC100001), Double-First Class University Plan (C176220100042), the Postgraduate Research and Innovation Foundation of Yunnan University (KC-23234662), and the Scientific Research Fund Project of Yunnan Provincial Department of Education (2023Y0210). The authors thank Advanced Analysis and Measurement Center of Yunnan University for the sample testing service.

Data availability

Data will be made available on reasonable request.

Declarations

Competing interests

All authors certify that they have no affiliations with or involvement in any organization or entity with any financial interest or non-financial interest in the subject matter or materials discussed in this manuscript.

Author details

¹Institute for Ecological Research and Pollution Control of Plateau Lakes, School of Ecology and Environmental Science, Yunnan University, Kunming 650504, China. ²Hubei Key Laboratory of Low Dimensional Optoelectronic Materials and Devices, Hubei University of Arts and Science, Xiangyang 441053, China. ³Faculty of Chemistry and Chemical Engineering, Yunnan Normal University, Kunming 650092, China. ⁴Key Laboratory of Coordination Chemistry of Jiangxi Province, School of Chemistry and Chemical Engineering, Jingtangshan University, Ji'an 343009, China.

Received: 11 August 2023 Revised: 15 November 2023 Accepted: 17

November 2023

Published online: 07 December 2023

References

- Arroyave JM, Avena M, Tan W, Wang M (2022) The two-species phosphate adsorption kinetics on goethite. *Chemosphere* 307:135782. <https://doi.org/10.1016/j.chemosphere.2022.135782>
- Canteral KFF, Dias YN, Fernandes AR (2023) Biochars from agro-industrial residues of the Amazon: an ecological alternative to enhance the use of phosphorus in agriculture. *Clean Technol Environ* 25(4):1119–1132. <https://doi.org/10.1007/s10098-022-02427-6>
- Canteral KFF, Dias YN, Fernandes AR (2023) Properties controlling phosphorus adsorption and stability in amazonian agro-industrial waste biochars: a multivariate approach. *Water Air Soil Poll* 234(6):376. <https://doi.org/10.1007/s11270-023-06386-6>
- Chen L, Li Y, Sun Y, Chen Y, Qian J (2019) La(OH)₃ loaded magnetic mesoporous nanospheres with highly efficient phosphate removal properties and superior pH stability. *Chem Eng J* 360:342–348. <https://doi.org/10.1016/j.cej.2018.11.234>
- Cheng P, Liu Y, Yang L, Ren Q, Wang X, Chi Y, Yuan H, Wang S, Ren Y-X (2023) Phosphate adsorption using calcium aluminate decahydrate to achieve low phosphate concentrations: batch and fixed-bed column studies. *J. Environ. Chem. Eng* 11(2):109377. <https://doi.org/10.1016/j.jece.2023.109377>
- de Carvalho Eufrásio Pinto M, David da Silva D, Amorim Gomes AL, Menezes dos Santos RM, Alves de Couto RA, Ferreira de Novais R, Leopoldo Constantino VR, Tronto J, Pinto FG (2019) Biochar from carrot residues chemically modified with magnesium for removing phosphorus from aqueous solution. *J Clean Prod* 222:36–46. <https://doi.org/10.1016/j.jclepro.2019.03.012>
- Demertzi M, Paulo JA, Arroja L, Dias AC (2016) A carbon footprint simulation model for the cork oak sector. *Sci. Total Environ.* 566–567:499–511
- Dong H, Wei L, Tarpeh WA (2020) Electro-assisted regeneration of pH-sensitive ion exchangers for sustainable phosphate removal and recovery. *Water Res* 184:116167. <https://doi.org/10.1016/j.watres.2020.116167>
- Erdogan FO (2019) Freundlich, Langmuir, Temkin, DR and Harkins-Jura Isotherm Studies on the adsorption of CO₂ on various porous adsorbents. *Int J Chem React Eng.* <https://doi.org/10.1515/ijcre-2018-0134>
- Feng Y, Luo Y, He Q, Zhao D, Zhang K, Shen S, Wang F (2021) Performance and mechanism of a biochar-based Ca-La composite for the adsorption of phosphate from water. *J Environ Chem Eng* 9(3):105267. <https://doi.org/10.1016/j.jece.2021.105267>
- Feng C, Zhang L, Zhang X, Li J, Li Y, Peng Y, Luo Y, Li R, Gao B, Hamouda MA, Smith K, Ali EF, Lee SS, Zhang Z, Rinklebe J, Shaheen SM (2023) Bio-assembled MgO-coated tea waste biochar efficiently decontaminates phosphate from water and kitchen waste fermentation liquid. *Biochar* 5(1):22. <https://doi.org/10.1007/s42773-023-00214-0>
- Feng W, Wang T, Zhu Y, Sun F, Giesy JP, Wu F (2023) Chemical composition, sources, and ecological effect of organic phosphorus in water ecosystems: a review. *Carbon Res* 2(1):12. <https://doi.org/10.1007/s44246-023-00038-4>
- Glemser O (1959) Structure of some hydroxides and hydrous oxides: binding of water in some hydroxides and hydrous oxides. *Nature* 183(4666):943–944. <https://doi.org/10.1038/183943a0>
- He Q, Zhao H, Teng Z, Wang Y, Sun W, Guo Y, Ji X, Hu W, Shiung Lam S, Li M (2023) Efficient recovery of phosphate by Fe₃O₄/La-MOF: an insight of adsorption performance and mechanism from electrochemical properties. *Sep Purif Technol* 314:123529. <https://doi.org/10.1016/j.seppur.2023.123529>
- Huang Y, He Y, Zhang H, Wang H, Li W, Li Y, Xu J, Wang B, Hu G (2022) Selective adsorption behavior and mechanism of phosphate in water by different lanthanum modified biochar. *J Environ Chem Eng* 10(3):107476. <https://doi.org/10.1016/j.jece.2022.107476>
- Huang K, Xia J, Lu Y, Zhang B, Shi W, Cao X, Zhang X, Woods LM, Han C, Chen C, Wang T, Wu J, Huang Y (2023) Self-reconstructed spinel surface structure enabling the long-term stable hydrogen evolution reaction/oxygen evolution reaction efficiency of FeCoNiRu high-entropy alloyed electrocatalyst. *Adv Sci* 10(14):2300094. <https://doi.org/10.1002/adv.202300094>
- Jia X, Wang H, Li Y, Xu J, Cheng H, Li M, Zhang S, Zhang H, Hu G (2022) Separable lanthanum-based porous PAN nanofiber membrane for effective aqueous phosphate removal. *Chem Eng J* 433:133538. <https://doi.org/10.1016/j.cej.2021.133538>
- Jia X, Zhao X, Bi Z, Zhang H, Huang S, Chun-Ho Lam J, Li W, Li Y, Wågberg T, Hu G (2023) Rod-shaped lanthanum oxychloride-decorated porous carbon material for efficient and ultra-fast removal of phosphorus from eutrophic water. *Sep. Purif. Technol* 306:122713. <https://doi.org/10.1016/j.seppur.2022.122713>
- Jia X, Zhao X, Zhou Y, Li F, Liu W, Huang Y, Zhang H, Ma J, Hu G (2023) Tri-functional lanthanum-based biochar for efficient phosphorus recovery, bacterial inhibition, and soil fertility enhancement. *Biochar* 5(1):16. <https://doi.org/10.1007/s42773-023-00216-y>
- Kong H, Wang J, Zhang G, Shen F, Li Q, Huang Z (2023) Synthesis of three-dimensional porous lanthanum modified attapulgite chitosan hydrogel bead for phosphate removal: performance, mechanism, cost-benefit analysis. *Sep. Purif. Technol* 320:124098. <https://doi.org/10.1016/j.seppur.2023.124098>
- Li M, Fan X, Mao Q, Li Q, Zhang X, He G, Zhang S, Zhang W (2021) The hollow core-shell ferric oxide entrapped chitosan microcapsules as phosphate binders for phosphorus removal in vitro. *Carbohydr Polym* 257:117621. <https://doi.org/10.1016/j.carbpol.2021.117621>
- Li M, Feng M, Guo C, Qiu S, Zhang L, Zhao D, Guo H, Zhang K, Wang F (2023) Green and efficient Al-doped LaFeAl_{1-x}O₃ perovskite oxide for enhanced phosphate adsorption with creation of oxygen vacancies. *ACS Appl Mater Interfaces* 15(13):16942–16952. <https://doi.org/10.1021/acsami.2c19513>
- Li S, Shao J, Ma B, Wu B, Hu C (2023) Oxygen defects of MgLa-LDH enhancing electrostatic attraction and inner-sphere complexation during phosphate adsorption from wastewater. *Chem Eng J* 464:142589. <https://doi.org/10.1016/j.cej.2023.142589>
- Liu J, Wang P, Wang H, Li C, Si X, Qi J, Cao J, Zhong Z, Fei W, Feng J (2019) Defect-rich heterogeneous MoS₂/NiS₂ nanosheets electrocatalysts for efficient overall water splitting. *Adv Sci* 6(14):1900246. <https://doi.org/10.1002/adv.201900246>
- Liu T, Chen X, Wang X, Zheng S, Yang L (2018) Highly effective wastewater phosphorus removal by phosphorus accumulating organism combined with magnetic sorbent MFC@La(OH)₃. *Chem Eng J* 335:443–449. <https://doi.org/10.1016/j.cej.2017.10.117>
- Liu X, Zong E, Hu W, Song P, Wang J, Liu Q, Ma Z, Fu S (2019) Lignin-derived porous carbon loaded with La(OH)₃ nanorods for highly efficient removal of phosphate. *ACS Sustain Chem Eng* 7(1):758–768. <https://doi.org/10.1021/acssuschemeng.8b04382>
- Liu G, Dai Z, Liu X, Dahlgren RA, Xu J (2022) Modification of agricultural wastes to improve sorption capacities for pollutant removal from water—a review. *Carbon Res* 1(1):24. <https://doi.org/10.1007/s44246-022-00025-1>
- Liu Z, Liu H, Zhang Y, Lichtfouse E (2023) Efficient phosphate recycling by adsorption on alkaline sludge biochar. *Environ Chem Lett* 21(1):21–30. <https://doi.org/10.1007/s10311-022-01527-5>
- Lu L, Na C (2022) Gibbsian interpretation of Langmuir, Freundlich and Temkin isotherms for adsorption in solution. *Phil Mag Lett* 102(7):239–253. <https://doi.org/10.1080/09500839.2022.2084571>
- Lürling M, Kang L, Mucci M, van Oosterhout F, Noyma NP, Miranda M, Huszar VLM, Waajen G, Marinho MM (2020) Coagulation and precipitation of cyanobacterial blooms. *Ecol Eng* 158:106032. <https://doi.org/10.1016/j.ecoleng.2020.106032>
- Mahata BK, Chang S-M, Bose P (2022) Bio-inspired phosphate adsorption by copper-decorated weak base anion exchanger. *Sep Purif Technol* 296:121339. <https://doi.org/10.1016/j.seppur.2022.121339>

- Moumen E, Bazzi L, El Hankari S (2022) Metal-organic frameworks and their composites for the adsorption and sensing of phosphate. *Coord Chem Rev* 455:214376. <https://doi.org/10.1016/j.ccr.2021.214376>
- Neolaka YAB, Lawa Y, Naat JN, Pau Riwu AA, Darmokoesoemo H, Supriyanto G, Holdsworth CI, Amenaghawon AN, Kusuma HS (2020) A Cr(VI)-imprinted-poly(4-VP-co-EGDMA) sorbent prepared using precipitation polymerization and its application for selective adsorptive removal and solid phase extraction of Cr(VI) ions from electroplating industrial wastewater. *React Funct Polym* 147:104451. <https://doi.org/10.1016/j.reactfunctpolym.2019.104451>
- Park JH, Ok YS, Kim SH, Cho JS, Heo JS, Delaune RD, Seo DC (2015) Evaluation of phosphorus adsorption capacity of sesame straw biochar on aqueous solution: influence of activation methods and pyrolysis temperatures. *Environ Geochem Hlth* 37(6):969–983. <https://doi.org/10.1007/s10653-015-9709-9>
- Sarkhot DV, Ghezzehei TA, Berhe AA (2013) Effectiveness of biochar for sorption of ammonium and phosphate from dairy effluent. *J Environ Qual* 42(5):1545–1554. <https://doi.org/10.2134/jeq2012.0482>
- Shan S, Wang W, Liu D, Zhao Z, Shi W, Cui F (2020) Remarkable phosphate removal and recovery from wastewater by magnetically recyclable La₂O₂CO₃/γ-Fe₂O₃ nanocomposites. *J Hazard Mater* 397:122597. <https://doi.org/10.1016/j.jhazmat.2020.122597>
- Shan S, Zhang T, Wang W, Liu D, Shi W, Cui F (2021) Magnetite/hydrated cerium(III) carbonate for efficient phosphate elimination from aqueous solutions and the mechanistic investigation. *Chem Eng J* 425:128894. <https://doi.org/10.1016/j.cej.2021.128894>
- Shi W, Fu Y, Jiang W, Ye Y, Kang J, Liu D, Ren Y, Li D, Luo C, Xu Z (2019) Enhanced phosphate removal by zeolite loaded with Mg–Al–La ternary (hydr) oxides from aqueous solutions: Performance and mechanism. *Chem Eng J* 357:33–44. <https://doi.org/10.1016/j.cej.2018.08.003>
- Sing KSW (1985) Reporting physorption data for gas/solid systems with special reference to the determination of surface area and porosity (recommendations 1984). *Pure Appl Chem* 57(4):603–619. <https://doi.org/10.1351/pac198557040603>
- Sun S, Gao M, Wang Y, Qiu Q, Han J, Qiu L, Feng Y (2021) Phosphate removal via biological process coupling with hydroxyapatite crystallization in alternating anaerobic/aerobic biofilter reactor. *Biores Technol* 326:124728. <https://doi.org/10.1016/j.biortech.2021.124728>
- Tao Y, Liu S, Dong S, Wang C, Qu T, Li S, Li L, Ma Z (2022) An in situ grown amorphous ZrO₂ layer on zeolite for enhanced phosphate adsorption. *RSC Adv* 12(26):16751–16762. <https://doi.org/10.1039/D2RA01967A>
- van Oosterhout F, Waajien G, Yasserli S, Manzi Marinho M, Pessoa Noyma N, Mucci M, Douglas G, Lürling M (2020) Lanthanum in Water, Sediment, Macrophytes and chironomid larvae following application of Lanthanum modified bentonite to lake Rauwbraken (The Netherlands). *Sci Total Environ* 706:135188. <https://doi.org/10.1016/j.scitotenv.2019.135188>
- Wang J, Kaskel S (2012) KOH activation of carbon-based materials for energy storage. *J Mater Chem* 22(45):23710–23725. <https://doi.org/10.1039/C2JM34066F>
- Wang Z, Shen D, Shen F, Li T (2016) Phosphate adsorption on lanthanum loaded biochar. *Chemosphere* 150:1–7. <https://doi.org/10.1016/j.chemosphere.2016.02.004>
- Wang L, Wang J, Yan W, He C, Shi Y (2020) MgFe₂O₄-biochar based lanthanum alginate beads for advanced phosphate removal. *Chem Eng J* 387:123305. <https://doi.org/10.1016/j.cej.2019.123305>
- Wang Q, Lai Z, Luo C, Zhang J, Cao X, Liu J, Mu J (2021) Honeycomb-like activated carbon with microporous nanosheets structure prepared from waste biomass cork for highly efficient dye wastewater treatment. *J Hazard Mater* 416:125896. <https://doi.org/10.1016/j.jhazmat.2021.125896>
- Wang Z, Li W, Zhu J, Wang D, Meng H, Wang H, Li J (2021) Simultaneous adsorption of phosphate and zinc by lanthanum modified zeolite. *Environ Technol Inno* 24:101906. <https://doi.org/10.1016/j.eti.2021.101906>
- Wang B, Zhang H, Xu Z, Xu Y, Hu X, Wang H, Wang C, Chen L (2022) La/Al engineered bentonite composite for efficient phosphate separation from aqueous media: Preparation optimization, adsorptive behavior and mechanism insight. *Sep Purif Technol* 290:120894. <https://doi.org/10.1016/j.seppur.2022.120894>
- Wang Y, Chen L, Jiang Y, Yang X, Dai J, Dai X, Dong M, Yan Y (2022) Salt sacrificial template strategy and in-situ growth of lamellar La(OH)₃ on a novel PVDF foam for the simultaneous removal of phosphates and oil pollution without VOCs emission. *Sep Purif Technol* 288:120681. <https://doi.org/10.1016/j.seppur.2022.120681>
- Wang J, Zhang G, Qiao S, Zhou J (2023) Comparative assessment of formation pathways and adsorption behavior reveals the role of NaOH of MgO-modified diatomite on phosphate recovery. *Sci Total Environ* 876:162785. <https://doi.org/10.1016/j.scitotenv.2023.162785>
- Wang Y, Yang X, Dai J, Yan Y, Jiang Y, Chen L (2023) 3D lanthanum modified cellulose aerogel based on filter paper with excellent adsorption performance for phosphate. *Cellulose*. <https://doi.org/10.1007/s10570-023-05494-0>
- Yin X, Li X, Petropoulos E, Feng Y, Yang B, Xue L, Yang L, He S (2022) Phosphate removal from actual wastewater via La(OH)₃-C₃N₄ adsorption: Performance, mechanisms and applicability. *Sci Total Environ* 814:152791. <https://doi.org/10.1016/j.scitotenv.2021.152791>
- Yu J, Xiang C, Zhang G, Wang H, Ji Q, Qu J (2019) Activation of lattice oxygen in LaFe (Oxy)hydroxides for efficient phosphorus removal. *Environ Sci Technol* 53(15):9073–9080. <https://doi.org/10.1021/acs.est.9b01939>
- Zhang X, Wang W, Shi W, He J, Feng H, Xu Y, Cui F, Wang C (2016) Carbon nanofiber matrix with embedded LaCO₃OH synchronously captures phosphate and organic carbon to starve bacteria. *J Mater Chem A* 4(33):12799–12806. <https://doi.org/10.1039/C6TA04364J>
- Zhang X, Elsayed I, Song X, Shmulsky R, Hassan EB (2020) Microporous carbon nanoflakes derived from biomass cork waste for CO₂ capture. *Sci Total Environ* 748:142465. <https://doi.org/10.1016/j.scitotenv.2020.142465>
- Zhang Y, Kong B, Shen Z, Qian J, Pan B (2021) Phosphorus binding by lanthanum modified pyroaurite-like clay: performance and mechanisms. *ACS ES T Eng* 1(11):1565–1575. <https://doi.org/10.1021/acsestengg.1c00218>
- Zhang C, Wang X, Wang X, Liu B (2022) Characterization of La–Mg-modified palygorskite and its adsorption of phosphate. *J Environ Chem Eng* 10(3):107658. <https://doi.org/10.1016/j.jece.2022.107658>
- Zhao S, Wang B, Gao Q, Gao Y, Liu S (2017) Adsorption of phosphorus by different biochars. *Spectrosc Lett* 50(2):73–80. <https://doi.org/10.1080/00387010.2017.1287091>

Submit your manuscript to a SpringerOpen® journal and benefit from:

- Convenient online submission
- Rigorous peer review
- Open access: articles freely available online
- High visibility within the field
- Retaining the copyright to your article

Submit your next manuscript at ► [springeropen.com](https://www.springeropen.com)